Paper No. 18

A STATISTICAL TECHNIQUE FOR DETERMINING RAINFALL OVER LAND EMPLOYING NIMBUS-6 ESMR MEASUREMENTS

E. Rodgers, *Goddard Space Flight Center,* H. Siddalingaiah, *Computer Sciences Corporation, Silver Spring, Maryland 20910,* A. T. C. Chang and T. Wilheit, *Goddard Space Flight Center, Greenbelt, Maryland.*

ABSTRACT

An empirical method has been employed to deliniate synoptic scale rainfall over land utilizing Nimbus–6 ESMR measurements.

INTRODUCTION

Savage et al. (1976) demonstrated theoretically that at 37.0GHz, the frequency at which the Nimbus–6 ESMR (ESMR–6) sensor measures upwelling radiance, the scattering by hydrometeors is strong enough to render a qualitative interpretation of rain over land. Furthermore, Weinman and Guetter (1977) demonstrated from theoretical considerations that the upwelling radiation at 37.0GHz emerging from hydrometeors is essentially unpolarized. This in contrast to wet land surface whose reduced emissivity (due to surface moisture) becomes highly polarized when viewed obliquely. Thus, it is reasonable to conclude from these theoretical considerations that rain over dry land surfaces can be at least qualitatively monitored employing 37.0GHz radiometer measurements from ESMR–6.

It is the purpose of this study to substantiate the above conclusions and to arrive at an algorithm which detects rain over land by statistically analyzing ESMR–6 data. This statistical analysis will be performed by first sampling three categories of ESMR–6 brightness temperatures (T_B's)(representing rain over land, wet land surfaces without rain, and dry land surfaces), then testing these populations for uniqueness, and finally developing a classification algorithm to delineate rain over land.

THE ESMR–6 SYSTEM

The ESMR–6 system flown aboard Nimbus–6 (Wilheit, 1975) receives the thermal radiation upwelling from the earth's surface and atmosphere in a 250MHz band centered at 37.0GHz. The antenna beam scans electrically in 71 steps an arc of 70° ahead of the spacecraft along a conical surface with a constant incidence angle of 50° to the earth's surface every 5.3 seconds with a nominal resolution of 20km crosstrack and 45km down track. The instrument measures both horizontal and vertical polarization components by using two separate radiometric channels. The data are calibrated using warm (instrument ambient) and cold (cosmic background) inputs to the radiometer. The T_B as observed from the satellite are dependent upon the emission from the earth's surface modified by the intervening

atmosphere. The emissivity, being a function of the dielectric constant, is variable over land surfaces (depending on vegetation, surface roughness, and soil moisture) and generally large (ca,.9). In a raining atmosphere, three constituents contribute to the absorption: molecular oxygen, water vapor, and liquid droplets. Water droplets are the only source of scattering at this frequency. Ice crystals are essentially transparent.

DATA SAMPLING

In order to develop an algorithm which classifies a given ESMR-6 instantaneous field of view (IFOV) as rain over land, dry land surface, or wet land surface, simultaneous ground stations and radar measurements of rain and ESMR-6 T_B were needed. Eight daytime synoptic scale rainfall cases over the Southeastern United States were used where surface rain rate data taken from stations reporting hourly rainfall amounts and from the WSR-57 radar coincided with the Nimbus-6 overpass to within 5 minutes. The surface temperature in each of these cases was not less than 5°C. Rain areas were sampled within areas delineated as rain by the WSR-57 radar (rain rates $\geq$ 2.5 mm hr^{-1}) and/or the station reporting hourly rainfall amounts. Wet land surfaces were sampled in areas where rain had fallen within 3 hours and upstream and adjacent to the raincells observed on the WSR-57 radar. Dry land surfaces were sampled over areas where rain had not fallen within a 24 hr. period previous to the Nimbus-6 pass.

STATISTICAL ANALYSIS

Figure 1 presents the scatter plot of the sampled data. The C's represent the mean points of the populations. Each of the frequency concentration ellipses encompasses 68 percent (one standard deviation) of the data from the respective populations. These ellipses reveal the extent of scattering of the data from each population, the correlation between the variables T_H and T_V in each population (the higher the correlation the larger the eccentricity of the ellipse), and the extent of overlap among the populations. It can be seen that the largest overlap is between the populations representing rain areas and wet land surfaces. This ambiguity may be attributed to the fact that an ESMR-6 IFOV (pixel) partially filled with moderate to heavy rain or completely filled with very light rain is influenced by the wet surface background and consequently produces a signature somewhat similar to that of wet land surfaces.

The three concurrent lines drawn in this figure are the Fisher discriminant lines. These lines separate two-by-two the ensemble of points representing rain over land, dry land surfaces, and wet land surfaces.

Table 1 shows the elementary statistics of the sampled data. It can be seen from Figure 1 and Table 1, that the T_B representing rain over land are colder than those representing dry land surfaces. However, this will not always be the case. Since the surface emission is given by ϵT_s (ϵ is the surface emissivity and T_s is the surface thermodynamic temperature), there is an influence of T_s on ESMR-6 measured dry land surface T_B. A decrease in T_s results in a decreased ESMR-6 T_B of dry land surfaces and consequently in the reduced T_B contrast between dry land surfaces and rain over land.

It can also be seen from this table that the difference in the means of the horizontal and vertical polarized T_B (6.5°K) representing rain over land is much smaller when compared to the corresponding mean difference (16.1°K) representing wet land surfaces. This in accordance with the theoretical findings that hydrometeors are not polarized (Weinman and Guetter, 1977) whereas wet land surfaces are highly polarized.

Table 1
Rain Over Land

	Rain Area		Dry Ground		Wet Soil	
Sample Size: N	216		189		66	
	T_{HR}	T_{VR}	T_{HD}	T_{VD}	T_{HW}	T_{VW}
Mean: μ	254.53	260.98	271.46	278.18	252.05	268.86
Standard Deviation: d	7.21	5.81	6.18	7.2	9.41	7.64
Sample Correlation Coefficient Between T_H And T_V: ρ	0.55		0.37		0.82	

Prior to employing these data for the development of classification algorithms, an examination was made to verify whether the three populations were statistically distinguishable from one another. To accomplish this, tests were carried out first to determine the significance of the differences between the means of any two classes and second to estimate the simultaneous confidence intervals for the differences of the means of any two populations. It was found that the differences between the means of any two classes were highly significant and that the probability that the mean vectors of any two populations coincide was less than 1 in 100. The simultaneous confidence intervals computed according to Scheffe's procedure showed that none of the intervals contained zero except the one for the differences between the means of horizontal polarized T_B's for wet land surfaces and rain over land. However, the three populations are distinguishable from one another when the dual polarization information is taken into account simultaneously. It should be noted that the lower bounds for the differences of the means of the T_B's for rain over land and wet land surfaces are very small when compared to those of the other two pairs of the populations. Hence, it will be more difficult to detect rainfall over land from wet land surfaces. Since the populations were found to be statistically distinguishable and satisfied the Gaussian frequency distribution, the Bayesian pattern recognition technique was employed to develop a classification algorithm to detect and delineate active rainfall areas from wet and dry land surfaces. (Rodgers, et al., 1978.)

ERROR ANALYSIS

An error estimate was made in order to evaluate the performance of the classification algorithm. The error rates were computed according to the asymptotic formulas given by Okamoto (1963). The results are seen in Table 2 which shows that the chances of incorrectly classifying wet or dry land surfaces as rain over land is nearly 23 percent. But when a given ESMR-6 pixel is classified as rain over land and each of the eight contiguous pixels clustered around it is also classified as rainfall over land, then the chance of misclassification of that central pixel is reduced to 7.7×10^{-6} percent assuming each pixel is independently classified. Table 3 displays the actual probabilities that the classification algorithm classifies the sampled data into various populations as indicated. The average accuracy is computed by taking the mean of the diagonal elements of the corresponding error matrices. The apparent average accuracy compares well with the estimated average.

Table 2
Probabilities of Misclassification: Theoretical Computation

Known \ Classified	Rain	Dry	Wet
Rain	77.15	6.66	16.19
Dry	6.67	82.08	11.25
Wet	16.28	11.29	72.43

Average Accuracy: 77.22 Percent

Table 3
Bayesian Classification Error Matrix

Known \ Classified	Rain	Dry	Wet
Rain	89.35	6.02	4.63
Dry	7.41	91.53	1.06
Wet	27.27	15.15	57.58

Average Accuracy: 79.49 Percent

ALGORITHM EVALUATION

A case not previously used was tested to verify qualitatively the performance of the Bayesian Classification algorithm. This case consisted of a synoptic scale rain pattern over the Southeastern United States (14 September, 1976) which was observed by the ESMR-6 sensor (surface thermodynamic temperature $\geqslant 15°C$). Rainfall as delineated by the WSR-57 radar and stations reporting hourly rainfall amounts is seen in Figure 2. The approximate time of the radar PPI images was 1630 GMT (within 5 minutes of the Nimbus-6 pass). The reporting times of the stations reporting rain amounts were 1500, 1600, and 1700 GMT. The shaded areas within the WSR-57 radar PPI range (46 km) are rain rates greater than 2.5 mm hr^{-1}. The radars were located at Waycross and Macon, Georgia; Charleston, South Carolina; and Wilmington and Cape Hatteras, North Carolina. Surface station data were taken at 1800GMT. Dots, together with the hourly amounts of rain (see model in figure) if any, denote hourly rainfall reporting stations.

The Bayesian classification map is seen in Figure 3. Areas of clouds delineated by the Nimbus-6 Temperature Humidity Infrared Radiometer (THIR) 11.5 μm channel (equivalent blackbody temperatures (T_{BB}) $\leqslant 270°K$) are shown on the map. Rain areas in the absence of clouds or in areas of low clouds are misclassifications. Only regions covered by clusters of contiguous pixels classified into a single individual class are shown, since the probability of misclassifying clusters is much less than that of a single pixel.

A comparison of Figure 2 with Figure 3 shows good agreement between areal distribution of ESMR-6 derived rain over land and observed rain (no attempt was made to verify wet surfaces areas). However, the classified area of rainfall over North Carolina and Southwestern Georgia is contrary to ground observations. The

rainfall indicated by ESMR-6 over North Carolina may be suspended liquid water in the clouds ahead of the rain area (the area of rain was moving NE towards North Carolina). On the other hand, the ESMR-6 delineated rain over Southwestern Georgia, which was upstream from the rain area, may be due to wet land surfaces produced by the rain that fell a few hours prior to the Nimbus-6 pass.

The Bayesian classification algorithm was applied to another case (1645GMT August 27,1976, surface thermodynamic temperatures $\geqslant 15°C$) over the same geographical area as the previous case in order to determine whether the surface characteristics (vegetation, soil moisture, and surface roughness) had influenced the classification algorithm performance in the previous case. During this period, the area in question was under the influence of a Bermuda high and there was only convective rainfall in the area, particularly along the Gulf States. Results showed that the only areas classified as rain over land were along the Gulf Coast. The regions in the previous case where the algorithm showed rainfall were classified as dry land surfaces. Hence, there was no influence of extraneous surface characteristics on the outcome of the previous case study.

However, contradicting results occurred when the Bayesian classification algorithm was applied to a night time Nimbus-6 pass over the same geographical area (0525GMT, September 13, 1976, surface thermodynamic temperature $\geqslant 15°C$) where there was no synoptic scale rainfall reported. Almost all pixels were classified by the algorithm as rain over land. Examining the ESMR-6 T_B showed that the temperatures were below 0°C. This anomaly may be attributed to the change in the surface emissivity caused by the presence of dew on the vegetation. Therefore, the pattern classification algorithm trained by data sampled from Nimbus-6 daytime passes can be employed only when dew is absent.

CONCLUSIONS

Statistical analyses were performed on the sampled ESMR-6 data for the purpose of detecting rainfall areas over land from dry and wet land surfaces. It was found from these studies that synoptic scale rainfall over land, where surface thermodynamic temperatures were greater than 5°C and the vegetation was bereft of dew, could indeed be delineated despite the large ESMR-6 IFOV. However, there was some ambiguity in distinguishing between rainfall areas and wet land surfaces.

REFERENCES

Duda, R. O. and P. E. Hart, 1973: Pattern Classification and Seen Analysis, pp. 10-36, John Wiley and Sons, New York, NY.

Okamoto, M., 1973: An Asymptotic Expansion of the Distribution of the Linear Discriminant Function. Ann. Math. Statist., 34, 1286-1301.

Rodgers, E. B., H. Siddalingaiah, A. T. C. Chang, and T. Wilheit, 1978: A Statistical Technique for Determining Rainfall Over Land Employing Nimbus-6 ESMR Measurements, NASA TM 79631, pp. 33.

Savage, R. C., P. J. Guetter, and J. A. Weinman, 1976: The Observation of Rain Clouds over Land in Nimbus-6 Electrically Scanned Microwave Radiometer (ESMR-6) Data. Preprint Vol. 7th Conf. on Aerospace and Aeronautical Meteorology and Symposium on Remote Sensing from Satellite, 131-136.

Weinman, J. A. and P. J. Guetter, 1977: Determination of Rainfall Distribution from Microwave Radiation Measured by the Nimbus-6 ESMR. J. Appl. Meteor., 16, 437-442.

Wilheit, T. T., 1975: The Electrically Scanning Microwave Radiometer (ESMR) Experiment. Nimbus–6 User's Guide NASA Goddard Space Flight Center, 87-108.

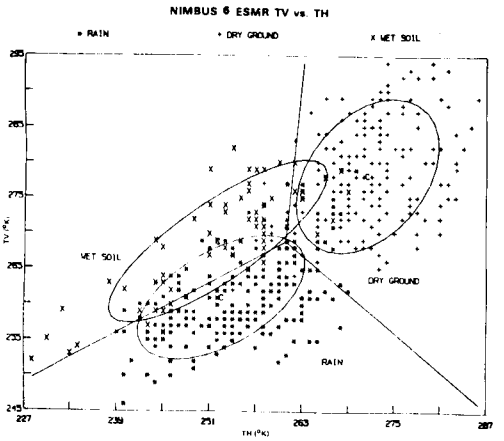

Fig. 1–Vertical polarized vs. horizontal polarized ESMR-6 T_B

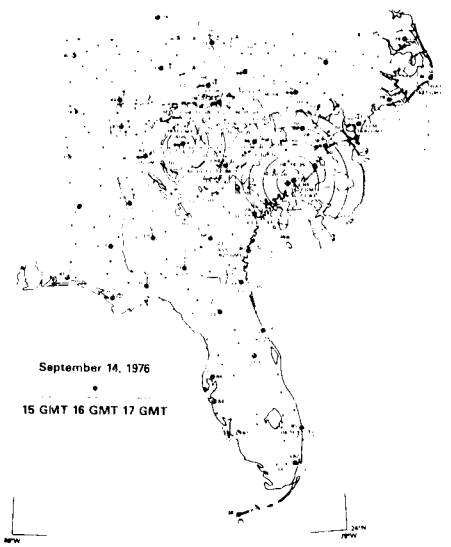

Fig. 2–Rainfall over the Southeast United States is delineated by the WSR-57 radar and hourly rainfall reporting station. Time of data is approximately 1630 GMT September 14, 1976. Shaded areas represent WSR-57 observed rain (rain rates $\geq$ 2.5 mm hr.). Dots represent hourly rainfall reporting stations.

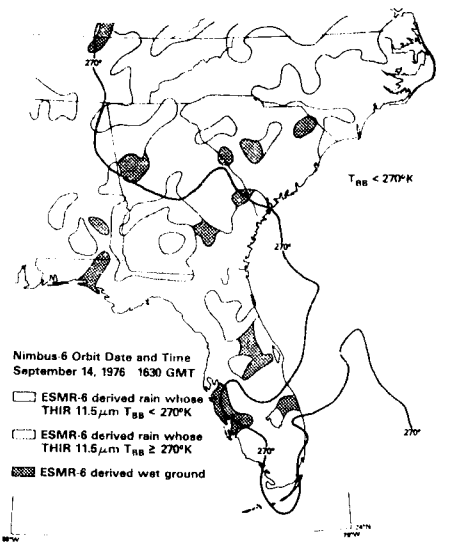

Fig. 3–ESMR-6 derived rainfall distribution using the Bayesian classifier. Dark curve depicts equivalent blackbody temperatures (T_{BB}) of 270° K as measured by the Nimbus–6 THIR 11.5 channel. Areas that have $T_{BB} \leq 270°K$ represent cloud cover. Time of Nimbus–6 pass 1630 GMT September 14, 1976.